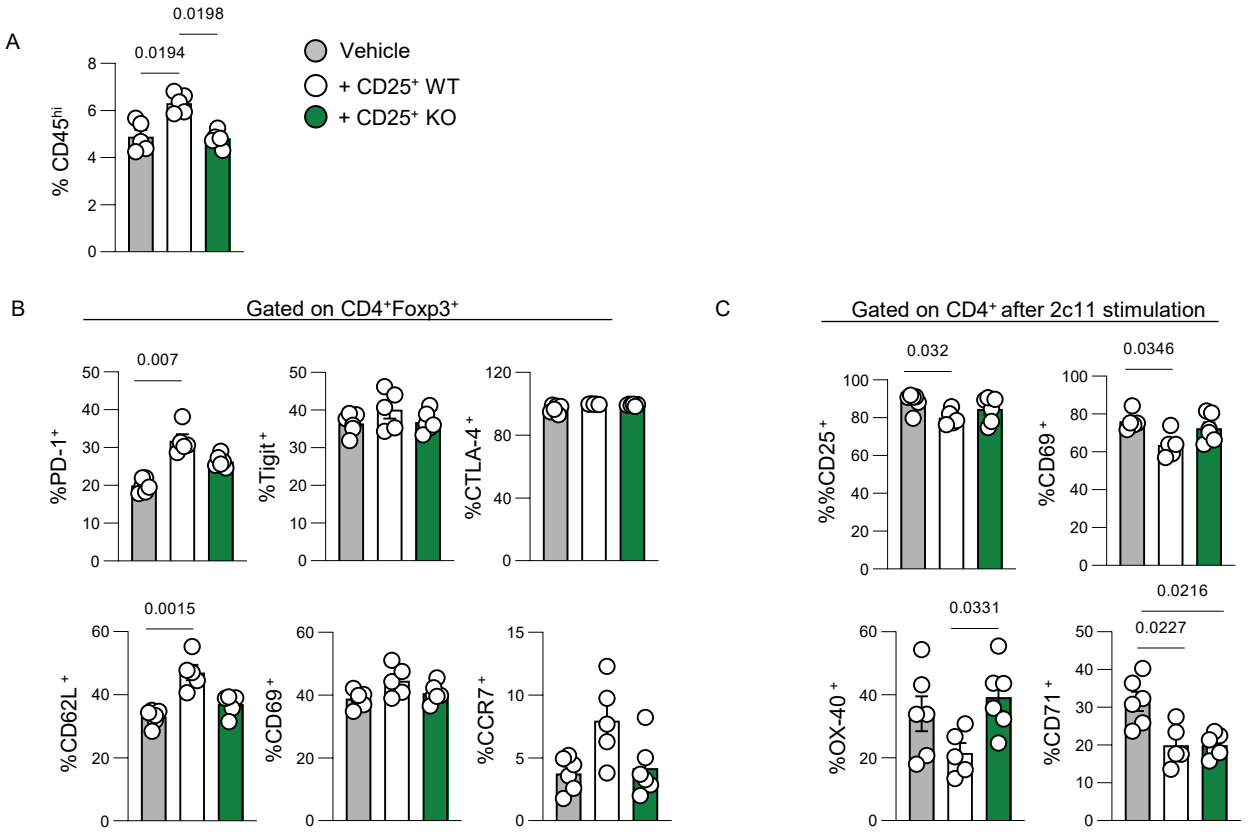

Supplementary Figure 1

A-B) Percentage of GFP$^+$/CD4$^+$ Tregs (A) and expression of Treg-specific markers (PD-1, Tigit, CTLA-4, CD62L, CD69, CCR7) in GFP$^+$/CD4$^+$ cells (B) from splenocytes isolated from EAE mice 20 days after MOG35-55 immunization. C) Expression of activation markers (CD25, CD69, OX-40, CD71) in CD4$^+$ T cells in splenocytes isolated from EAE mice and in vitro stimulated with 2C11 (polyclonal stimulation), 20 days after MOG35-55 immunization. N=4-10/ group; data are presented as mean +/- SEM. Statistical analysis has been performed with one- way Anova Kruskal Wallis test (A-C).

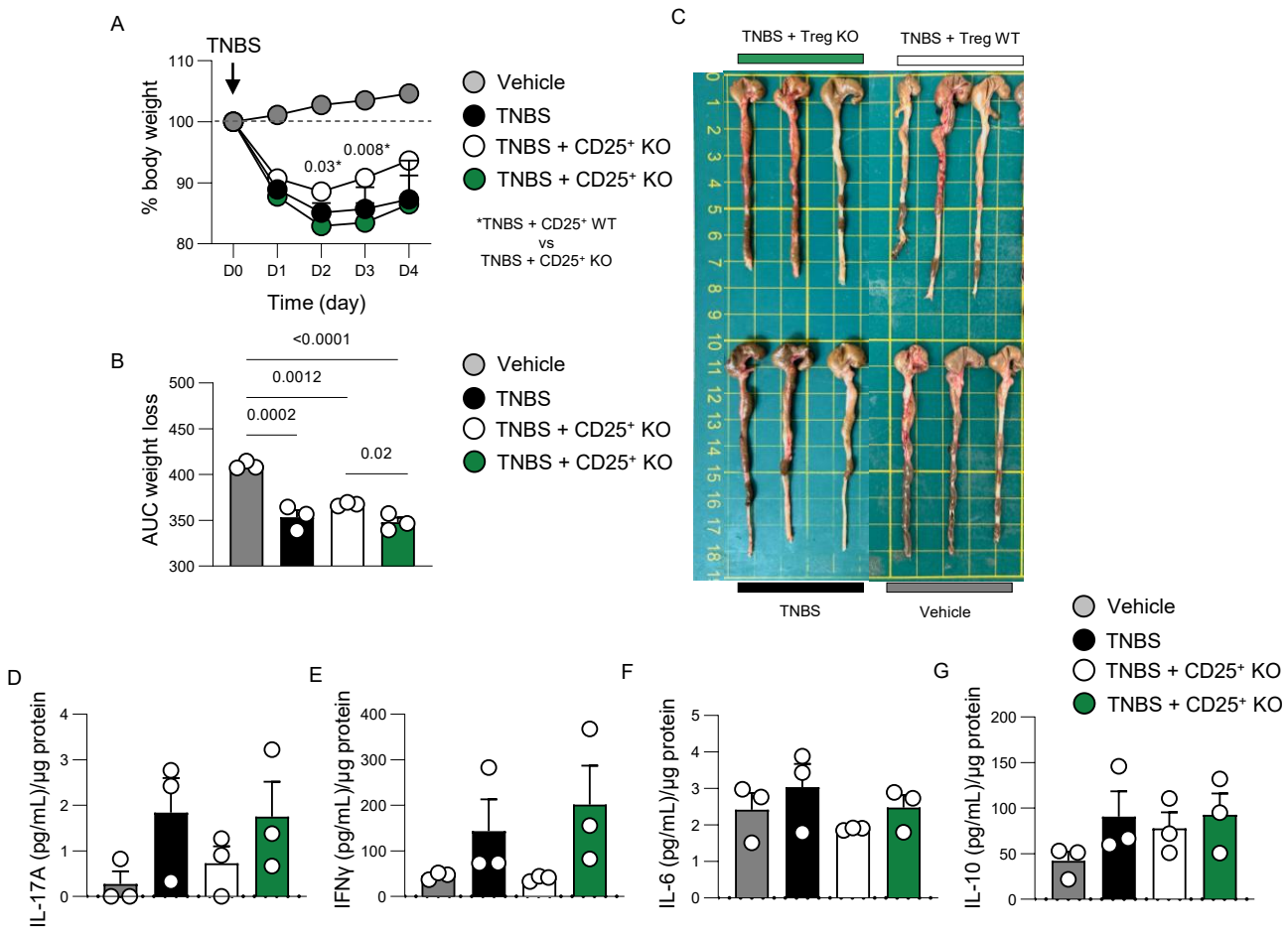

Supplementary Figure 2

A) Percentage of body weight reduction in mice undergoing TNBS-induced colitis with or without the administration of WT or KO Tregs, compared to control mice receiving vehicle. Body weight was taken before TNBS administration (day 0) and for the following 5 days; B) area under the curve of the percentage of body weight reduction; C) representative pictures of colons from experimental groups after 5 days from TNBS administration; D-G) Quantification of pro-inflammatory cytokines (IL-17A, IFN**γ**, IL-6) and anti-inflammatory (IL-10) from the colons of experimental mice. N=3/group; data are shown as mean +/- SEM. Statistical analysis was performed with one-way Anova (A-B, D-G).

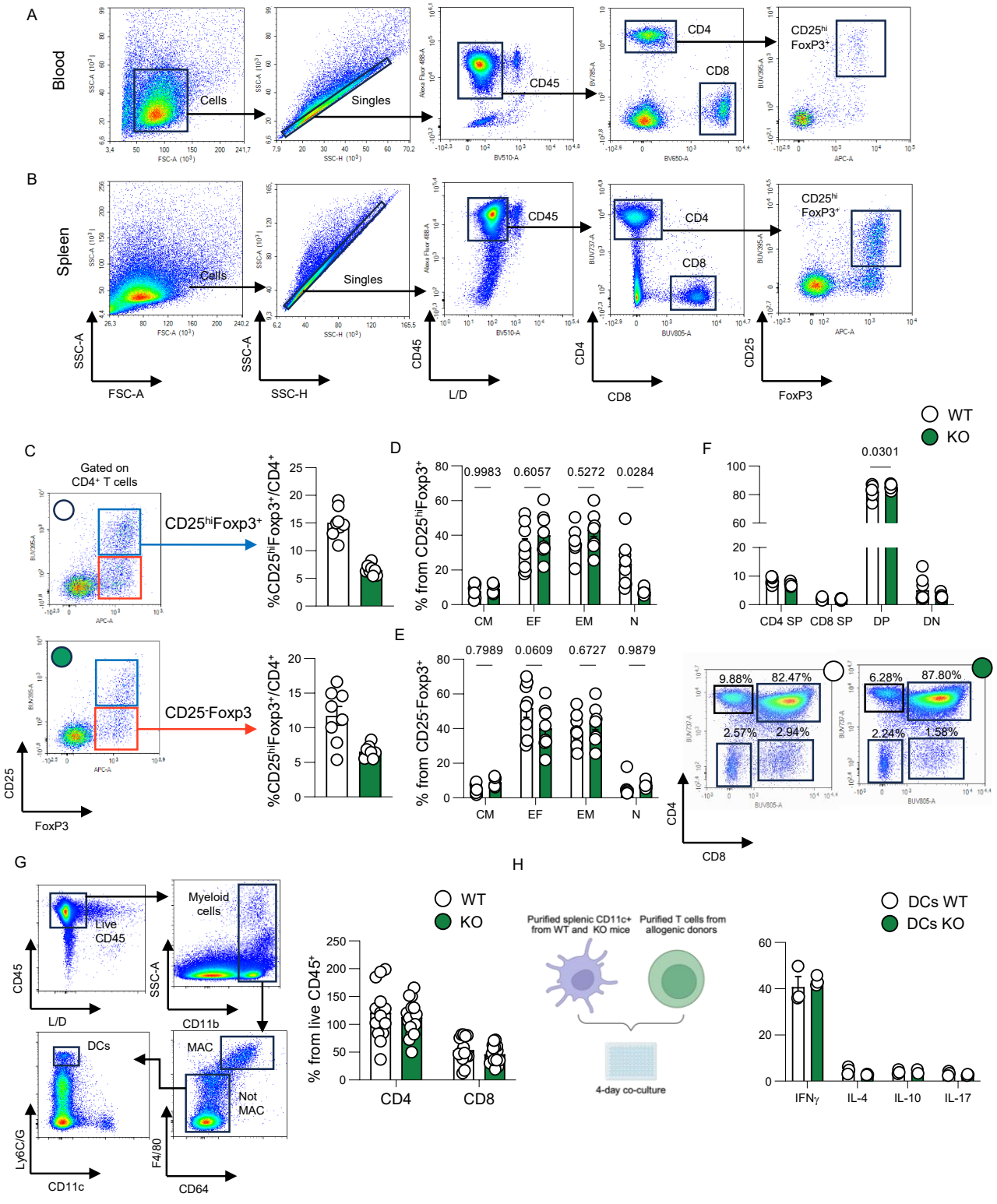

Supplementary Figure 3

A-B) Gating strategy for Treg identification by flow cytometry in the circulation (A) and spleens (B) of *Srebp1c* KO and WT mice. Cells were gated according to dimension based on FSC-A and SSC-A, singles discriminated by SSC-A vs SSC-H gating and within this population live leukocytes identified as CD45+ and live/dead staining (L/D) negative. Helper and cytotoxic T cells were identified by the expression of CD4 and CD8 markers,

respectively, and within CD4 T cells, Tregs were identified as CD25hi FoxP3+. Frequency of CD4 and CD8 single and double positive or negative cells. Representative density plots from flow cytometry analysis are reported. C) Representative plots and frequency of CD25hiFoxP3+ and CD25-FoxP3+ Tregs in the spleen from *Srebp1c* WT and KO mice. D-E) Frequency of central memory (CD62L+CD44+, CM), effector (CD62L-CD44-, EF), effector memory (CD62L-CD44+, EM), and naïve (CD62L+CD44-, N) within CD25hiFoxP3+ (D) and CD25-FoxP3+ (E) Tregs in the spleen of *Srebp1c* WT and KO mice. F) Frequency of CD4 and CD8 single and double positive or negative cells. Representative density plots from flow cytometry analysis are reported. G) Gating strategy for dendritic cells (DCs) and macrophages (Mac) identification in the spleens of *Srebp1c* KO and WT mice. Live leukocytes were identified as CD45+ and L/D- cells, and within this population, myeloid cells were distinguished by CD11 b expression. Within CD11b+, macrophages were identified by the expression of F4/80 and CD64 (Mac), while in the non-Mac population, DCs were gated as CD11c+ Ly6C/G- cells. Percentage of DCs and Mac out of live leukocytes (CD45) from the spleens of *Srebp1c* KO and WT mice. H) Schematic representation of a mixed lymphocyte reaction between DCs, purified as CD11c+ from the spleen of *Srebp1c* KO and WT mice, and T cells isolated from the spleens of allogenic donors (CBA mice) cultured for 4 days. Cytokine production (IFNγ, IL-4, IL-10 and IL-17) was measured by flow cytometry after re-stimulation with PMA/ionomycin in the presence of brefeldin (4 h). N=3-8/ group; data are presented as mean +/- SEM. Statistical analysis was performed with two-way Anova (C, D, E) and unpaired non-parametric T test (F, G).

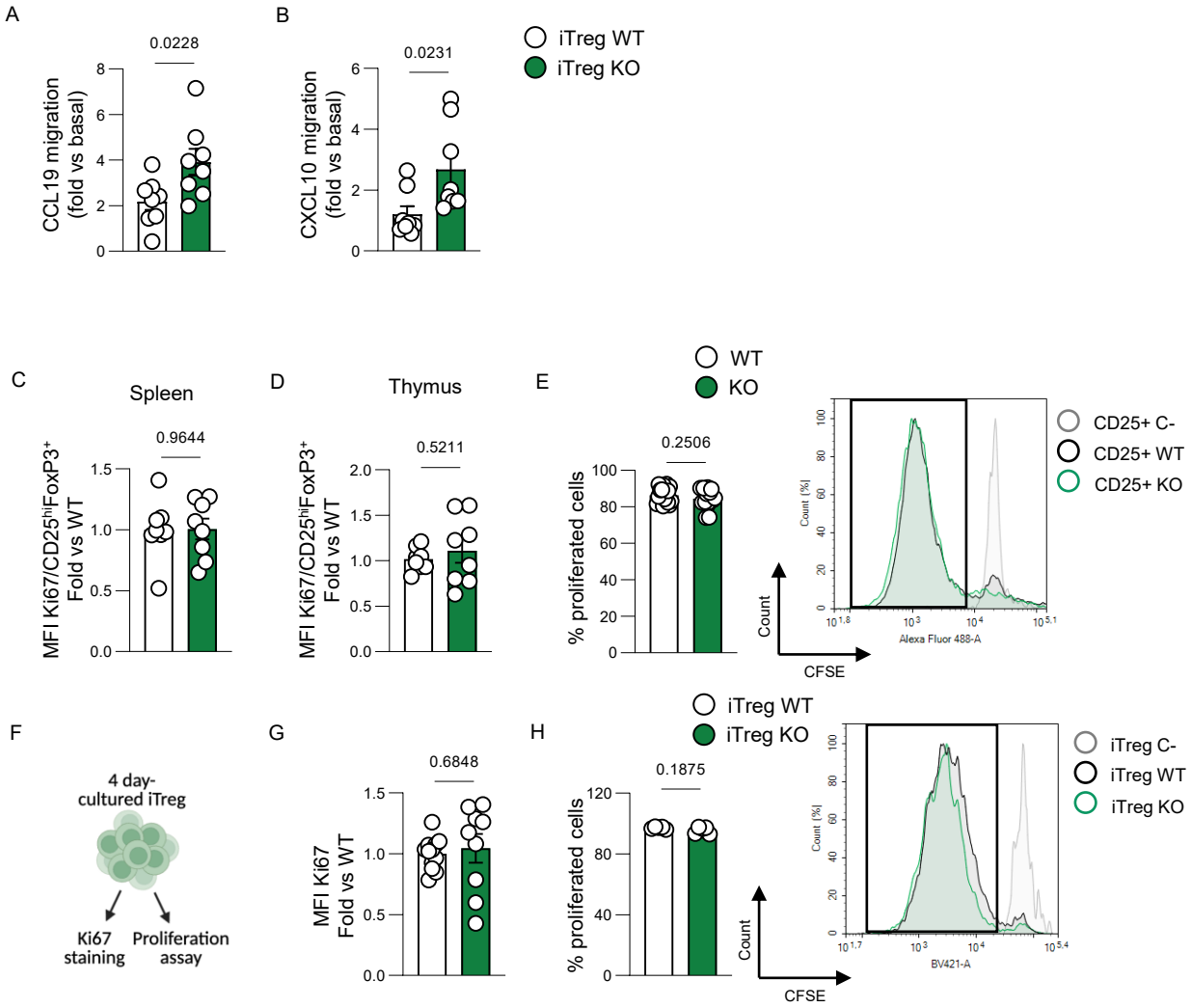

Supplementary Figure 4

A-B) In vitro migration assay of in vitro generated Tregs (iTregs) from WT and *Srebp1c* KO mice toward CCL19 (A) and CXCL10 (B) chemokines after 3 hours of incubation in 24-well plate transwells. Results are corrected versus spontaneous (basal) migration toward the medium. C-D) Mean fluorescence intensity (MFI) of Ki67 in CD25hiFoxP3+/CD4+ cells from the spleen (C) and thymus (D) of *Srebp1c* WT and KO mice. Values are corrected for WT values and represent two independent experiments (n=4/group). E) Proliferation of freshly isolated CD4+CD25+ Tregs by CFSE dilution. 0,15 x 10^6 cells were cultured for 4 days in anti-CD3/CD28 (0.25 µg/mL) coated 96-well plate. Proliferation was measured by flow cytometry and quantified as the percentage of cells with reduced CFSE fluorescence (black square) relative to the unstimulated negative control (C-). Values represent three independent experiments (n=4-5/group). F) Graphic representation of the experimental approaches used to test iTreg proliferation. G) Mean fluorescence intensity (MFI) of Ki67 in *Srebp1c* WT and KO iTregs. Data are corrected on WT values. H) Proliferation of iTregs by TraceViolet dilution. 0,15 x 10^6 cells were cultured for 4 days in anti-CD3/CD28 (0.25 µg/mL) coated 96-well plate. Proliferation was measured by flow cytometry and quantified as the percentage of cells with reduced TraceViolet fluorescence (black square)

relative to the unstimulated negative control (C-). N=4-12/group; data are presented as mean +/- SEM. Statistical analysis was performed with unpaired non-parametric T test (A-E, G, H).

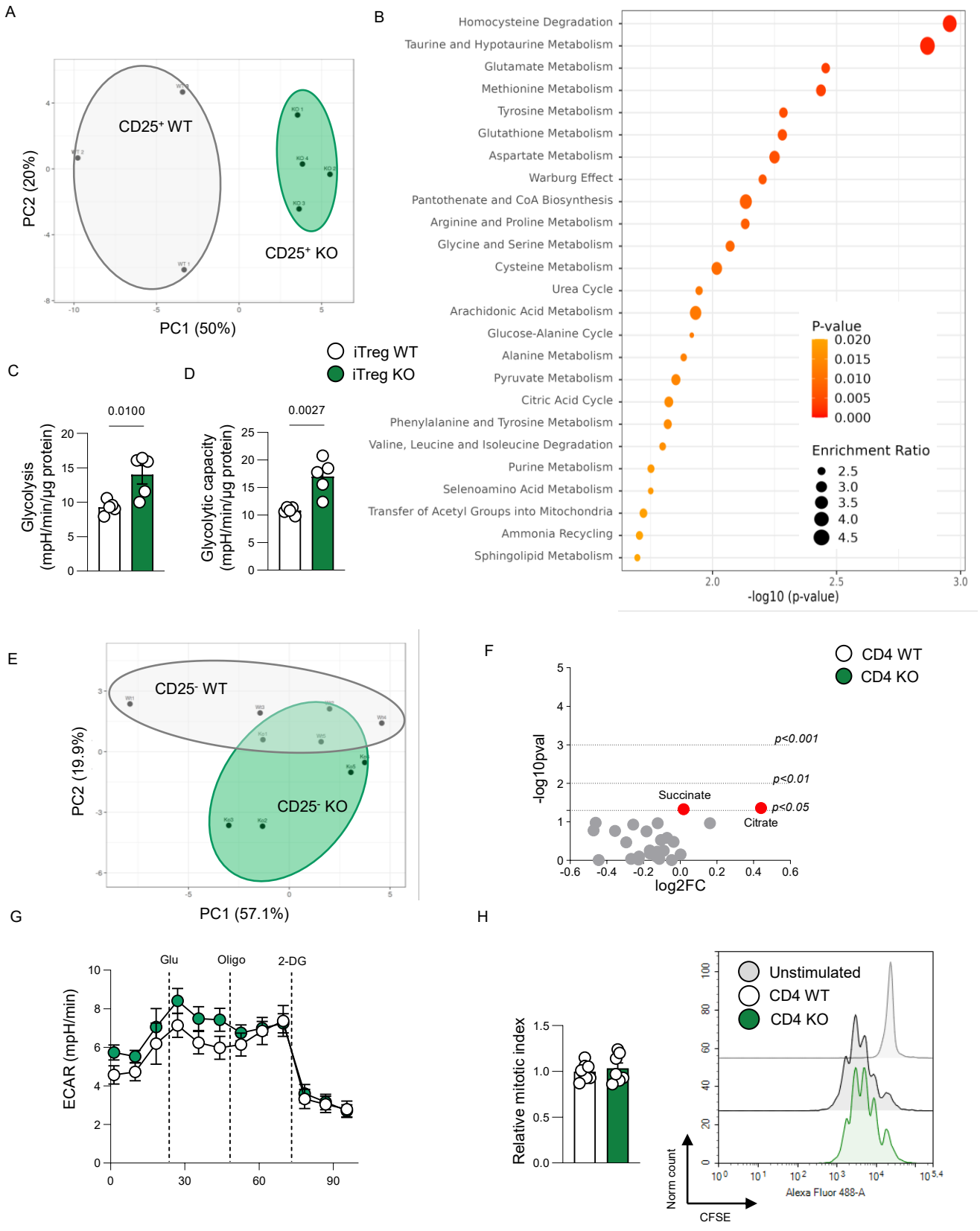

Supplementary Figure 5

A) PCA analysis from targeted metabolomics of Srebp1c WT and KO CD25+ Tregs. B) Top 25 significant pathways (-log10 p-value>1.3) from Metabolite Set Enrichment Analysis (MSEA) of significantly different

metabolites performed by MetaboAnalyst® from targeted metabolomics of WT and *Srebp1c* KO CD25+ Tregs. C-D) Glycolysis (C) and Glycolytic capacity (D) measured by Glucose stress test tested by Seahorse® on iTregs from *Srebp1c* WT and KO mice. E) PCA analysis from targeted metabolomics of Srebp1c WT and KO CD4+ CD25- T conventional cells. F) Volcano plot from targeted metabolomics of Srebp1c WT and KO CD4+ CD25- T conventional cells. G) ECAR analysis from glucose stress test tested by Seahorse on Srebp1c WT and KO CD4+ CD25- T conventional cells. H) Proliferation of CD4 T cells after CD3/CD28 stimulation for 4 days. Data are presented as relative mitotic index compared to WT cells. N=3-8/ group; gata are presented as mean +/- SEM. Statistical analysis was performed with unpaired non-parametric T test (C, D, H).

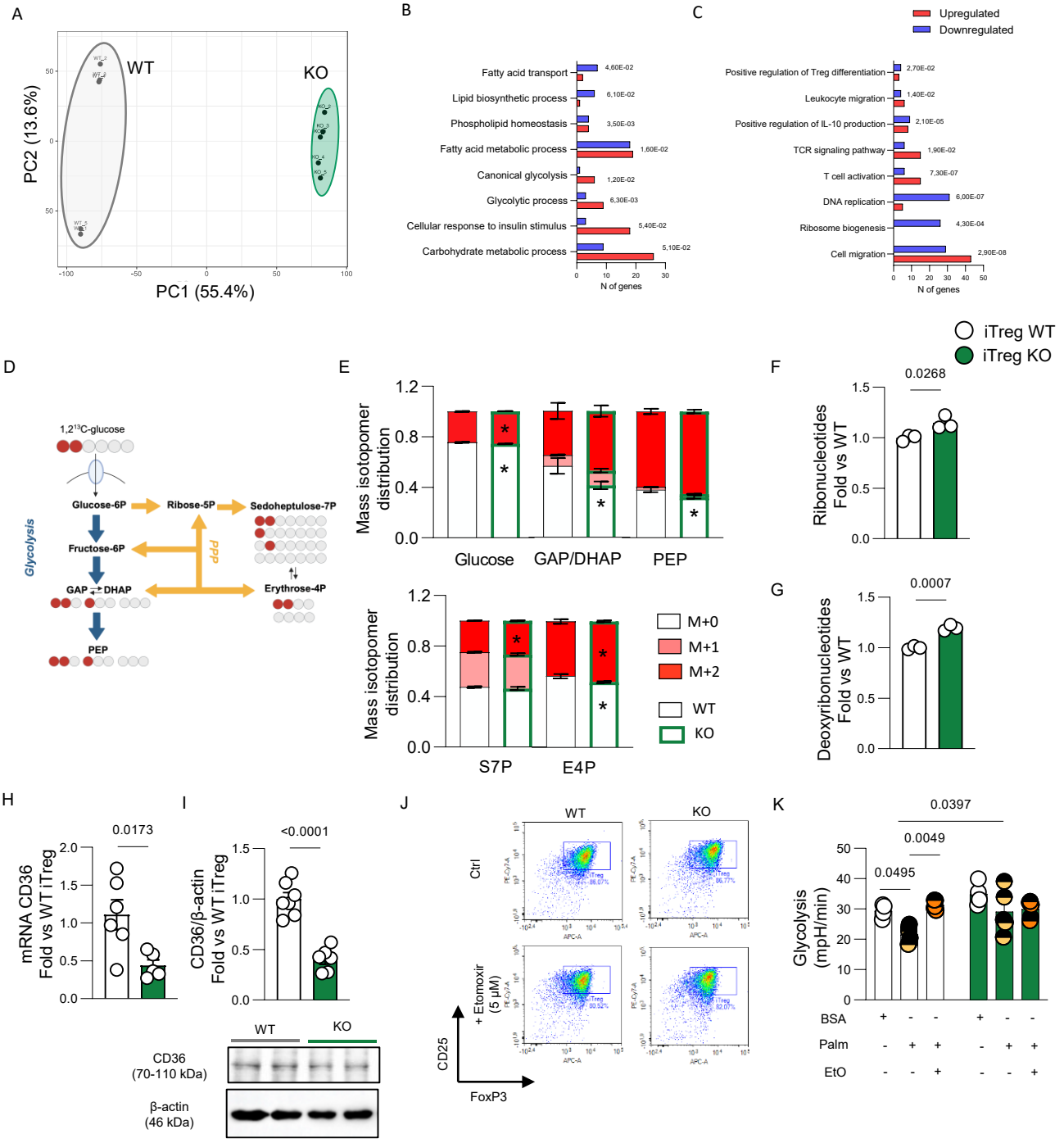

Supplementary Figure 6

A) Principal component analysis (PCA) from RNA-seq of *Srebp1c* WT and KO iTregs. B-C) Gene ontology (GO) terms of Biological Processes (BP) from David database analysis of DEGs from RNA-seq of *Srebp1c* KO vs WT iTregs, showing the number of upregulated (red) and downregulated (blue) genes for each pathway and its pValue. Histograms show the most affected pathways related to metabolism and energy (B) and to Treg function and activation (C). D) Graphic representation of labeled metabolites of glycolytic and PPP pathway detected after incubation of iTregs for 2h with DMEM medium reconstituted with 5mM of "cold" glucose and 5mM of [1,2-

C13] D-glucose. E) Mass topoisomer distribution (1, M1, or 2, M2, labeled carbons) after analysis of 1,2C-glucose fluxes of Glucose, Dihydroxyacetone phosphate/Glyceraldehyde 3-phosphate (DHAP/GAP), phosphoenolpyruvate (PEP), erithrose-4-phosphate (E4P), sedoheptulose-7-phosphate (S7P) in *Srebp1c* KO vs WT iTregs. F-G) Sum of ribonucleotides (J) and deoxyribonucleotides (K) normalized on WT measured by metabolomics of Srebp1c KO and WT iTregs. H-I) Gene expression by RT-qPCR (D) and protein quantification by western blot analysis (E) of CD36 in WT and *Srebp1c* KO iTregs; representative pictures from western blot analysis for CD36 are presented. J) Representative density plots of CD25 and FoxP3 expression from flow cytometry analysis of *Srebp1c* WT and KO iTregs in the presence or absence of etomoxir (5 μM for 4 hours). K) Glycolysis (mpH/min) analyzed by Seahorse® Glucose Stress Test assay tested in iTregs from WT and *Srebp1c* KO pre-incubated with BSA, palmitate (100 μM for 30 minutes) or palmitate + etomoxir (5 μM for 4 hours). N=5 biological replicates/ group (A-C), 3-7 (E-I, K); data are presented as mean +/- SEM and statistical was performed with unpaired non-parametric Ttest (E-I) and two-way Anova (K).

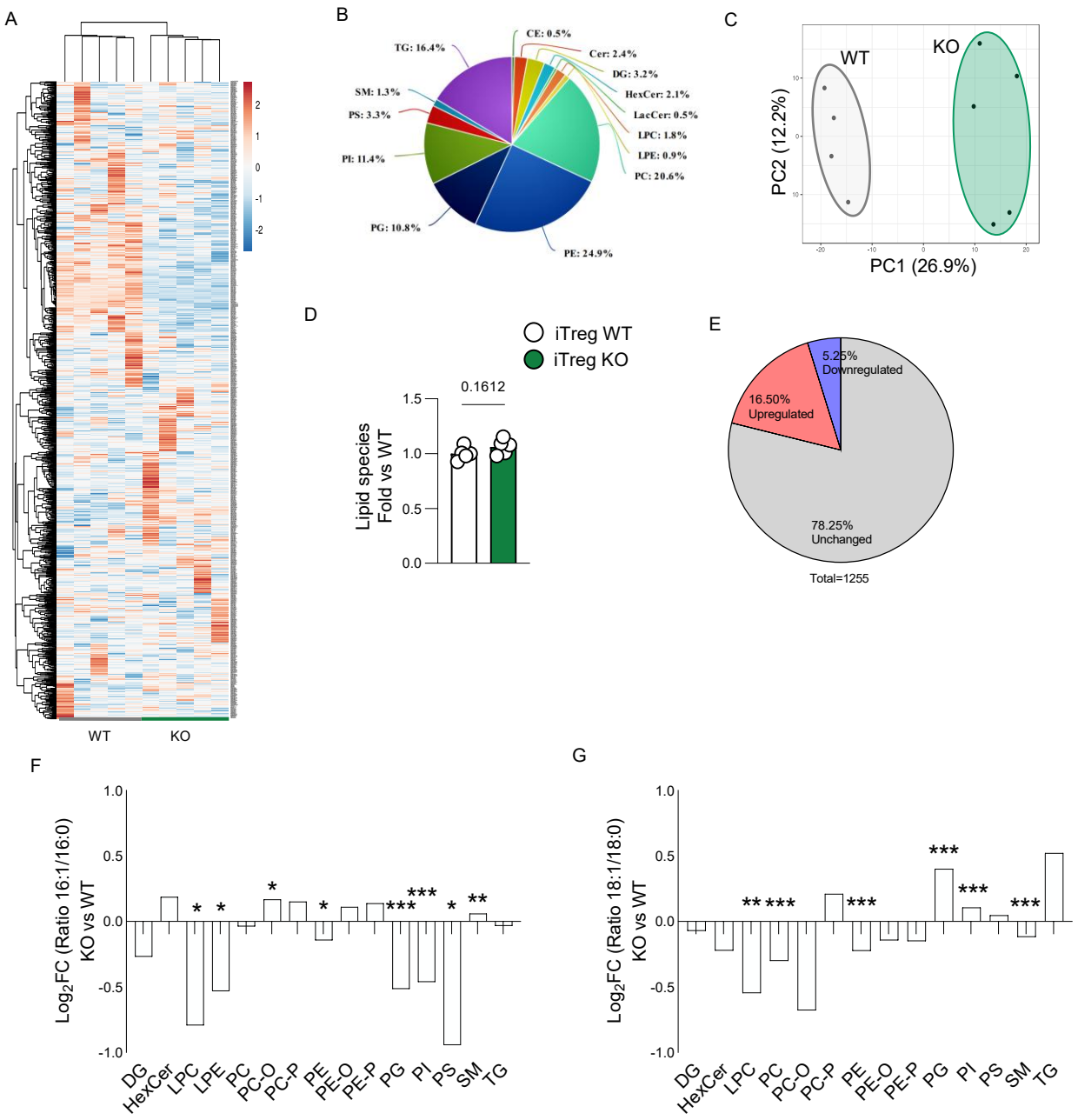

Supplementary Figure 7

A) Heatmap from lipid species analysis from lipidomics of *Srebp1c* KO and WT iTregs. B) Most abundant lipid classes identified by lipidomic analysis of iTregs from WT and *Srebp1c* KO mice. C) PCA analysis from lipidomic analysis of iTregs from WT and *Srebp1c* KO mice (5 biological replicates/group). D) Sum of all lipid species detected by lipidomics in Srebp1c WT and Ko iTregs, normalized on WT mean. E) Distribution of significantly increased lipid species (16,50%) and decreased (5,22%) on total lipid species identified (1255). F-G) Log_2FC of the ratio between 16:1/16:0 (F) and 18:1/18:0 (G) of the main lipid classes identified by lipidomics (DG, HexCer, LPC, LPE, PC, PC-O, PC-P, PE, PE-O, PE-P, PG, PI, PS, SM and TG) in *Srebp1c* KO iTregs compared to WT.

Lipidomics was performed on 5 biological replicates/group. In panel D data are presented as mean +/- SEM and statistical analysis was performed with unpaired non-parametric T test.

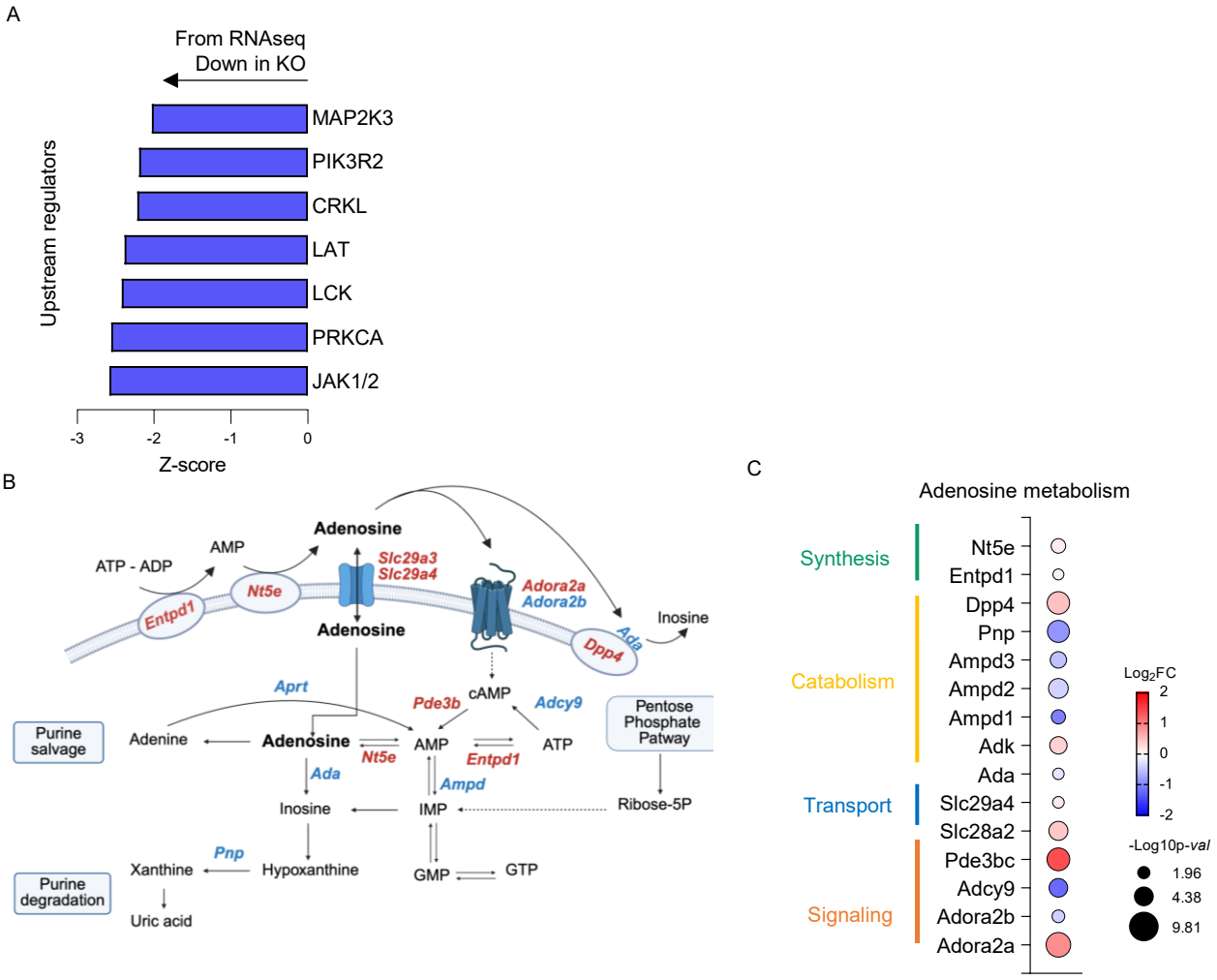

Supplementary Figure 8

A) Upstream regulators associated with intracellular signaling and cytokine pathways predicted down-regulated (negative z-score, blue) by IPA® software from RNA-seq of WT vs Srebp1c KO iTregs. B) Graphic representation of adenosine metabolism consisting of extracellular ectonucleotidases, transporters, intracellular metabolic enzymes and adenosine receptors that together control its production, uptake and intracellular signaling. In more details, Nt5e (CD73) converts AMP to adenosine; Entpd1 (CD39) hydrolyzes ATP and ADP to AMP, supplying substrate for CD73; Dpp4 (CD26) binds ADA and modulates extracellular adenosine clearance; Pnp cleaves purine nucleosides; Ampd1/2/3 deaminate AMP to IMP; Adk phosphorylates adenosine to AMP; Ada deaminates adenosine to inosine; Slc29a4 (ENT4) mediates bidirectional, pH-sensitive uptake of adenosine; Slc28a2 (CNT2) imports adenosine into cells; Pde3b hydrolyzes cAMP to AMP; Adcy9 generates intracellular cAMP from ATP downstream of Gs signaling; Adora2a is a high-affinity Gs-coupled extracellular adenosine receptor; Adora2b is a lower-affinity Gs-coupled

extracellular adenosine receptor activated at higher adenosine concentrations. C) Expression of genes related to adenosine synthesis, catabolism, transport, and signaling from RNA-seq on *Srebp1c* KO and WT iTregs. Dimension of the bubble represents the $-\log_{10}$ pValue, while the color represents the $\log_2$FC compared to WT (in blue downregulated and in red upregulated genes). RNA-seq was performed on 5 biological replicates/group.

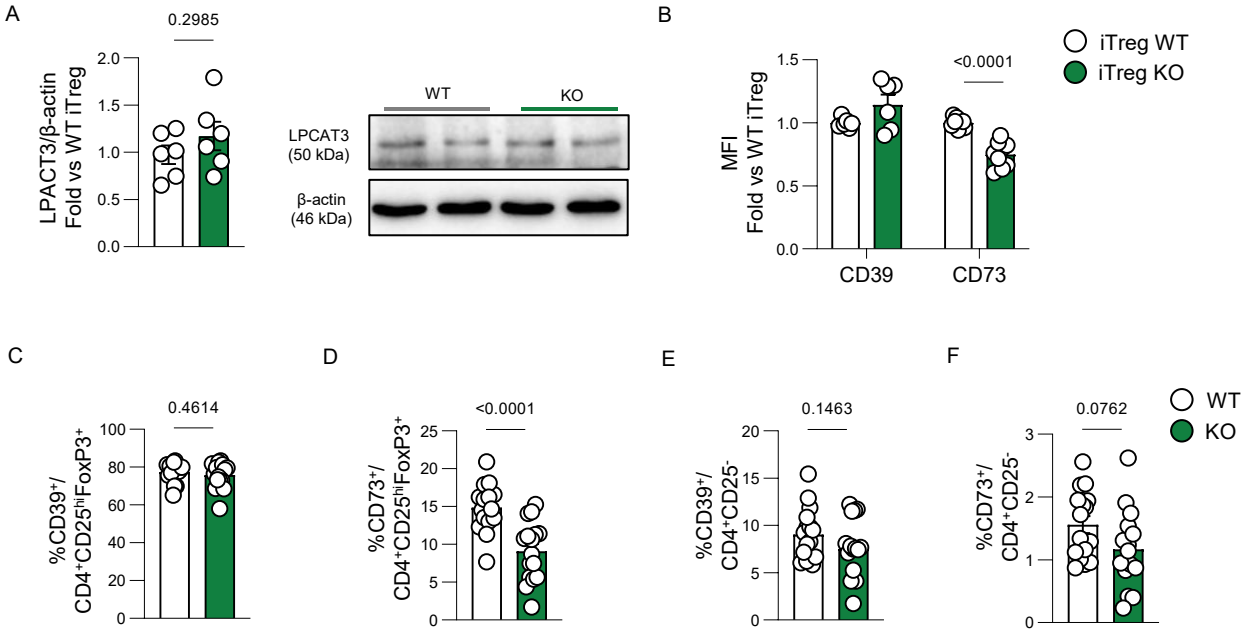

Supplementary Figure 9

A) Quantification of LPCAT3 by Western Blot analysis of *Srebp1c* WT and KO iTreg. Data are corrected on β-actin abundance; a representative western blot for LPCAT3 and β-actin is shown. B) Expression of CD39 and CD73 by flow cytometry in *Srebp1c* WT and KO iTregs. Data are expressed as a fold change of mean intensity fluorescence (MFI) compared to WT. C-D) Expression of CD39 (C) and CD73 (D) by flow cytometry in CD4+CD25hi FoxP3+ Tregs from the spleen of *Srebp1c* WT and KO mice. E-F) Expression of CD39 (E) and CD73 (F) by flow cytometry in CD4+CD25- T conventional cells from the spleen of *Srebp1c* WT and KO mice. N=5-16/ group; data are presented as mean +/- SEM. Statistical analysis was performed with unpaired non-parametric T test (A, B-F).